Submitted to "Engineering Geology'' **(first-revised version)**

Swelling behavior of compacted bentonite-sand mixture during water infiltration

Abhishek Rawat[1*], Wiebke Baille[1], Snehasish Tripathy[2]

Chair of Foundation Engineering Soil and Rock Mechanics, Ruhr-Universität Bochum, 44801, Germany.

[2] Geoenvironmental Research Centre, School of Engineering, Cardiff University, Cardiff, UK.

Number of words: 7749

Number of Tables: 2

Number of Figures: 13

***Corresponding author**

Abhishek Rawat

Gebäude IC 5/115, Universitätsstraße 150, 44780 Bochum, Germany

E-Mail: abhishek.rawat@rub.de

ABSTRACT

A laboratory-based water infiltration test was conducted with compacted Calcigel bentonite-sand mixture (50:50) at room temperature to mimic the transient hydration of a backfill material in nuclear waste repository conditions. The test was performed with an innovative column-type experimental device, which facilitated the continuous and non-destructive measurements of temperature, relative humidity, water content and total stresses in both axial and lateral direction at various preselected locations along the height of soil sample. The effect of groundwater geochemistry on the bentonite hydration process was not considered in this study. The distilled water was supplied from the bottom-end under 15-kPa hydration pressure for a period of 349 days to mimic the water ingress from the host rock. The test results highlighted the hydration-induced heterogeneity in the material and its effect on the lateral swelling pressure development along the height of soil sample. The axial swelling pressure measurements revealed the factors, which affect the stress-transfer mechanism between both the ends. The simultaneous measurements of relative humidity and water content indicated the porosity redistribution close to the hydration-end during the test.

Keywords

Bentonite-sand mixture, coupled hydro-mechanical behavior, backfill material, swelling pressure, nuclear waste repository.

1. Introduction

In Germany, a bentonite-sand mixture (50:50) compacted to bricks is proposed to use as a backfill material in nuclear waste repositories for long-lived radioactive wastes (Rothfuchs et al., 2005; Jobmann et al., 2015, 2017). As a primary function, backfill material creates a low permeable zone for delaying the water ingress from the near-field biosphere towards the waste canister. In the early stage of hydration, the external part of material hydrates first and fills the available constructional gaps. Once the existing constructional gaps are filled, the swelling pressure develops in both lateral and axial directions under a constant volume condition. For the mechanical stability of the entire disposal system, the rate of saturation and the resulting swelling pressure are crucial from the design point of view. Hence, an understanding of the coupled hydro-mechanical behavior of backfill materials is paramount for ensuring long-term safety.

In this regard, several full-scale experiments have been performed under repository-relevant boundary conditions (e.g., Alonso et al., 2005; Gens et al., 2009; Villar et al., 2014). For instance, a Full-scale Engineered Barriers Experiment (FEBEx) was commissioned at the Grimsel underground research laboratory in Switzerland (Alonso et al., 2005), whereas a laboratory-based full-scale mockup experiment was performed as a forerunner of the FEBEx field-scale test (Martín and Barcala, 2005). In another example, the Engineered-Barrier (EB) experiment was conducted at Mont Terri Underground Research Laboratory in Switzerland, starting in October 2000. The test run under isothermal conditions (average temperature 16 °C) for 10.5 years, where the granular backfill and the compacted bentonite blocks were subjected to the artificial hydration in year 2002 to mimic the water ingress from host rock. The dismantling of test started on October 2012 to

investigate the state of backfill materials under the applied hydration (Villar et al., 2014). Apart from the initial installation cost, the laboratory-based mockup tests have certain advantages over the field-scale experiments, such as a precise control over the applied thermal/hydraulic gradient, an efficient data monitoring, and a reasonable testing period.

Several reduced-scale mockup tests have been performed using the column-type testing devices (e.g., Cuevas et al., 1997; Yong et al., 1997; Börgesson et al., 2001; Pintado et al., 2002; Gatabin and Billaud, 2005; Villar et al., 2005; Åkesson et al., 2009; Schanz et al., 2013; Saba et al., 2014; Tripathy et al., 2015). In the column-type testing concept, the barrier and backfill materials are subjected to repository relevant thermal and hydraulic gradients under K0-condition. The time history of temperature, relative humidity, and the mechanical response (swelling pressure) of the materials are monitored with an elapsed time. The swelling pressure is usually measured at the low temperature end, whereas the water content, volumetric, and chemical properties of the tested materials are determined after termination of the tests (Villar et al., 2005; Tripathy et al., 2015). For instance, Saba et al. (2014) conducted two small-scale mock-up tests (dia. = 60 mm; height = 118 mm) under constant volume condition. The results highlighted the anisotropic swelling behavior and the dependency of radial swelling pressure kinetics on the distance from the hydration end. The test results were discussed based on the relative humidity measurements, which were performed in the separate test during the transient hydration of same material (Wang et al., 2013).

The magnitude of swelling pressure that is developed during the transient hydration process depends upon the saturation rate (i.e., water content and relative humidity distribution) and the

stiffness of the boundary (restraint), that may differ in both axial and lateral directions. Therefore, an understanding of the coupled hydro-mechanical behavior of compacted expansive soil-based materials demands measurements of the axial total stresses at both ends, the lateral stress, and simultaneous measurements of the water content and relative humidity. These aspects have not been explored in detail in the past. In this regard, a water infiltration test was conducted with compacted Calcigel bentonite-sand mixture (50:50) at room temperature. The geochemical aspects of clay-water interactions was not considered in this study. Hence, the distilled water was supplied from the bottom-end under 15-kPa hydration pressure to mimic the water ingress from the host rock. The test was performed with an innovative column-type experimental device, which facilitated the continuous and non-destructive measurements of temperature, relative humidity, water content and total stresses in both axial and radial direction at various preselected locations along the height of soil sample. The test was conducted for a period of 349 days.

2. Material

The investigated material was the compacted mixture of Calcigel bentonite and sand with equal dry mass ratio (50:50). Calcigel is a commercially available bentonite from the southern part of Germany with 60-70 % montmorillonite. It has a liquid limit of 180 %, plastic limit of 43-45 % and specific gravity of 2.80. The cation exchange capacity (CEC) is 74 meq/100 gm with 67 % of Ca^{+2} as a predominant exchangeable cation. Table 1 summarizes the relevant geotechnical properties of the tested materials. The Calcigel powder has 6 % hygroscopic moisture content. Prior to prepare a mixture with oven-dried medium sand (DIN 18123), the required volume of water was added to sand to achieve the mixture water content equal to 9 %. This method of

preparing the moist mixture gives less lump formations in the bentonite. Later, the moist-mixture was stored in a sealed plastic bag and kept in an airtight container for homogeneous moisture distribution for a period of 28 days.

3. Experimental methods

3.1 Column-type Experimental Set-up

Figure 1 shows constructional details of the newly designed column-type test device. The device is comprised of top and bottom plugs (items 1 and 5 in Fig. 1a), sample rings (items S1, S2, and S3 in Fig. 1a), and a confining cell (item 8). A rigid frame (item 9) provides the restraint along the axial direction. The stresses in the axial direction are measured using the load cells (items 6 and 7). The test set-up allows testing a cylindrical soil samples (dia. = 150 mm and height = 300 mm) and provides three measurement sections located at various heights from the bottom of the sample, such as X1 (50 mm), X2 (150 mm), and X3 (250 mm) (Fig. 1a).

The top and bottom plugs have similar constructional features for applying the thermal and hydraulic gradients along the height of soil sample. The plug contains porous stainless-steel base (dia. = 150 mm and thickness = 10 mm), and a metallic chamber (dia. = 150 mm and thickness = 20 mm). The porous base has a water inlet and an air outlet that can be used in case of thermo-hydraulic tests. The metallic chamber accommodates the heating/cooling coil, which in turn is connected to an external thermostat (not shown). The heating/cooling temperature is controlled by circulating silicon oil in the coil with the precision of 0.1 °C. The integrated design of the metallic

chamber with a porous base provides an adequate thermal equilibrium between the heating and hydration systems. These plugs transfer the axial total stress to the top and bottom load cells through a Polyvinylidene fluoride (PVDF) cylindrical piston (dia. = 148 mm and height = 100 mm). PVDF is a non-reactive thermoplastic and provides suitable thermal insulation for the heating unit (thermal conductivity = 0.13 W/m.K).

To accommodate soil sample, three PVDF sample rings (outer dia. = 350 mm, inner dia. = 150 mm, and height = 100 mm) are used (i.e., S1, S2, and S3) (Fig. 1). The PVDF sample rings assembly provide the mechanical stability, an adequate thermal insulation in the lateral direction, and accommodates the ports for the components of the monitoring sensors. Compacted soil samples can be prepared by compacting soil-water mixtures within each sample ring and further placed within the device. Each sample ring has four holes at the mid height, but radially positioned at an angle of 90° for installing the sensors that facilitate measuring temperature, relative humidity, water content, and lateral total stress (Fig. 1b). The sensors are installed with their respective PVDF adaptors (Fig. 1c) for minimizing the heat loss and any possible disturbances to the electronics of the sensors. The provision of O-ring connections along with tightening screws that are made of PVDF provide the air/water tight joints between two consecutive sample rings (Fig. 1a). A stainless-steel confining cell is used to provide additional resistance against the outward lateral deformation of the sample rings during a test (Fig. 1a). Additionally, the confining cell facilitates the installation of the lateral load cells (Fig. 2). A vertical stain-less steel plate provides a restraint for the lateral load cells (Fig. 2b). Table 2 shows the type of sensors and the instruments used with the device. For each case, the measurement range and accuracy are shown.

3.2 Sample preparation and test procedure

An initial dry density of 1.80 Mg/m^3 with 6 to 9 % initial water content is proposed for the compacted bentonite-sand bricks as a backfill material according to the German reference concept for the disposal of long-lived radioactive waste (Rothfuchs et al., 2005; Jobmann et al., 2015, 2017). In this regards, the mixture of Calcigel bentonite-sand with 9 % initial water content was compacted in three layers using uniaxial static compaction under 30 MPa in the vertical direction. During the compaction process, the surface of the compacted layer was scarified prior to place the next layer to ensure a proper homogeneous connection. The initial suction was measured using the chilled mirror hygroscope (26.9 MPa). After the compaction, the compacted block was extruded from the mould, the achieved mean dry density was 1.85 Mg/m^3 (block dia. = 153 mm; height = 100 mm). Total three blocks were compacted to achieve the required overall sample height of 300 mm. It should be noted here that the compacted sample exhibited post-compaction strains during the extrusion process. Consequently, the sample diameter was slightly larger than the inner diameter of sample rings (i.e., 150 mm). Hence, these blocks were prepared for installing inside the sample ring with monitoring sensors after the extrusion from the mould. For installing the Time Domain Reflectometry (TDR) based soil moisture measuring sensors, two parallel holes were drilled (dia. = 3.5 mm; length = 110 mm). Additionally, two holes were drilled for inserting the Pt100 sensor (dia. = 6 mm; length = 10 mm) associated with VAISALA relative humidity sensor and an independent Pt100 sensor (dia. = 3 mm; length = 10 mm). For the installation of KYOWA miniature pressure transducers, a seating space was created during the compaction process using stainless steel dummy having dimensions identical to KYOWA pressure transducer. Figure 3 shows the compacted block with seating space for the installation of the KYOWA pressure

transducer. The TDR-based water content measuring probe consists of two parallel wave-guides made of stainless steel (dia. = 3.5 mm; length = 110 mm). These wave-guides have a polyvinyl chloride coating for waterproofing. For a precise water content measurement, these wave-guides must be embedded completely inside the soil sample. These wave-guides are sensitive to deformation without any change in the measurement. The volume fraction of the embedded sensors was 0.14 % of the total sample volume (six Pt100 sensors, three TDR probes and two miniature pressure transducers). Hence, the sensor's embedment has insignificant effect on the sample response during the hydration under the confined conditions.

The test was conducted under a constant volume condition at room temperature; the air outlet at the bottom plug was kept closed, while the air outlet at top plug was kept open to evacuate the air during the hydration process. The site-specific ground water was replaced with the distilled water and supplied from the bottom-end under 15-kPa hydration pressure to mimic the water ingress from the host rock. Sensors along with data logger continuously monitored temperature, relative humidity, water content and total stress in both axial and lateral directions. The test was conducted for a period of 349 days. For the post-experimental measurements, the soil samples were collected from different locations along the height during the dismantling of test set-up. The relative humidity was measured using the chilled mirror technique, whereas the water content was measured following the standard oven-drying method.

4. Results

Figure 4a presents the relative humidity (RH) evolution over elapsed time for measurement

sections X1, X2, and X3. The post-experimental measurements are also shown in the figure. The initial relative humidity of soil sample (i.e., 81.5 %) captured by the RH probes agreed well with the measured value (i.e., 81 %) using the chilled mirror technique. The RH measurements at section X1 exhibited a sharp increase before reaching to 95 % in 45 days. With further hydration, the relative humidity increased gradually to 98.3 % in 120 days and latter remained almost constant. A similar trend can be observed for measurement sections X2 and X3. The measured values increased linearly before reaching to 95 % at X2 and 93 % at X3 in 349 days.

Figure 4b presents the evolution of water content with elapsed time at sections X1, X2 and X3 along with the post-experimental measurements. Similar to the relative humidity evolution at section X1, the water content increased rapidly before reaching to 13.8 % in 45 days. With further hydration, the water content at section X1 gradually increased to 17 % in 105 days and latter remained almost constant. The measurements at section X2 and X3 exhibited a lower incremental rate, particularly for section X3. The measured water content at section X2 reached to 13 % in 349 days. On the other hand, the measured water content at section X3 increased to 10.8 % from an initial value of 9 % in 349 days. The evolution of water content showed that the measured water content at X1 (13.8 %) was higher than the measured one at section X2 (13 %) at the same relative humidity level (95 %) or total suction (7 MPa).

Based on the transient relative humidity measurements along with the measured temperature, soil total suction (s) can be computed using Kelvin's equation:

$$s = -\left(\frac{\rho_w RT}{M_w}\right) ln\left(\frac{RH(\%)}{100}\right) \qquad (1)$$

where ρ_w is the water unit mass (1 Mg/m^3); R is the universal (molar) gas constant (8.31432 J/mol

K); T is the absolute temperature (°K), equal to (273.15 + $t_{measured\ (°C)}$); M_w is the molecular mass of water vapour (18.016 kg/kmol) and RH is the relative humidity in (%).

Fig. 5a presents soil total suction evolution over elapsed time for measurement sections X1, X2 and X3 along with the post-experimental measurements. The total suction decreases rapidly close to hydration end (i.e., at the measurement section X1) and reaches to 7 MPa within 45 days. From this point, the total suction decreases gradually and reaches 2.43 MPa 349 days. On the other hand, the total suction at section X2 and X3 exhibit successive decrease to 7 MPa and 10.54 MPa within 349 days, respectively.

The degree of saturation values during the transient hydration process were deduced from the water content measurements by assuming a constant void ratio (i.e., 0.47) along the height of soil sample. However, the assumption is not valid in case of expansive soils due to their swelling and collapse behavior during the hydration. Figure 5b shows the evolution of degree of saturation for three measurement sections. The initial degree of saturation was close to 0.51 for sample having approximately 9 % initial water content and a global void ratio of 0.47 along the height. The section X1 achieved 95 % saturation in 87 days and 100 % saturation in 142 days. Later, the computed degree of saturation values greater than 1 was observed at section X1. While the sample away from hydration end remained in the unsaturated state within the entire testing period. The sample achieved close to 75 % and 60 % saturation at measurement sections X2 and X3 after 349 days of hydration, respectively.

Figure 6a presents the axial total stress evolution over the elapsed time; the transient axial

stress measurements were performed at the top and bottom ends of the sample using load cells and the KYOWA miniature pressure transducers. The KYOWA miniature pressure transducers were installed between two compacted blocks (i.e., 100 mm and 200 mm from the bottom end). Prior to initiate the test, an initial siting stress of 50-60 kPa was applied during the installation of the test set-up to ensure a proper connection between the sample and top/bottom load cells. With the initiation of hydration, the bottom load cell responded quickly and reached to 1.1 MPa within 45 days. After time t = 45 days, the axial total stresses measured at the bottom end increases gradually before reaching 1.68 MPa within 349 days. The measured axial total stress at the top-end was lower than the measured one at the bottom end for a testing period of 238 days as shown by a point P in Fig. 6a. The KYOWA miniature pressure transducer has 4.15E-4 m^2 pressure sensing area and 1 MPa rated capacity. These sensors were installed in a seating-space in the compacted block as depicted in Fig. 3a. The measurements revealed that these sensors may have some initial gap between the pressure-sensing surface and the upper compacted block; this may be due to improper installation. The measurements show that these sensors respond when the hydration front reaches to the zone of their seating-space, the pressure transducer close to the bottom block at B1 reaches to 1 MPa within 105 days. Whereas the sensor close to top block at B2 reaches to 1 MPa within 285 days.

Figure 6b presents the evolution of lateral total stress at measurement sections X1, X2 and X3. In the present test, a cylindrical piston and load cell assembly measured the total stress in the lateral direction at section X1, X2 and X3. During the installation of test set-up, these pistons were kept in contact with the sample by applying some nominal siting stress. With the initiation of hydration from the bottom-end, the lateral total stress increased rapidly and exhibited higher values

as compared to the measured axial total stresses with the top and bottom load cells. The measurements at section X1 showed a rapid increase and reached to 2.18 MPa in 45 days. With the further hydration, the measured values at X1 showed some oscillations before reaching to a value of 2.13 MPa in 349 days. The measurements at X2 showed a lower incremental rate as compared to the measured values at X1. The lateral stress at section X2 increased asymptotically and reached to 3.76 MPa in 349 days. On the other hand, the measured lateral stress at section X3 increased linearly during the entire testing period. The experimental results clearly exhibit the effect of distance from the hydration end on the lateral swelling pressure dynamics. The lowest rate of increase was observed at the farthest measurement section X3.

5. Discussion

The water infiltration test mimics the transient hydration of compacted bentonite-sand mixture (50:50) as a backfill material at the nuclear waste repository. The test was performed for a period of 349 days. The transient measurements revealed that the sample did not achieve full saturation within the testing period. The evolution of state variables (measured and computed) and the measured axial and lateral total stress developed by the sample during the hydration highlighted the key features of material swelling behavior under an applied hydraulic gradient. The post-experimental measurements revealed the hydration induced heterogeneity along the height of soil sample. To explain the swelling response of compacted bentonite-sand mixture under the repository relevant scenarios, the test results are discussed in three subsections, such as:

- Evolution of state variables,
- Material swelling behavior, and

- Water retention behavior.

5.1 Evolution of state variables

In the present test, the liquid water was supplied from the bottom-end under 15-kPa hydration pressure. The bottom-most layer of sample (in contact with the saturated porous stone) attained saturation immediately after the initiation of hydration. Pusch (2001) investigated the effect of an applied hydration pressure on the extension of the wetting zone in the highly compacted blocks of MX80 bentonite (dry density = 1.51 Mg/m^3) by injecting liquid water under a pressure of 0.650 MPa through a perforated injection pipe for 3 and 20 minutes. The test result revealed that the applied hydration pressure affected the rate of saturation only up to 10 mm distance from the injection point. In the present case with the applied hydration pressure of 15-kPa, the water migration took place due to the water potential gradient along the height of soil sample, which was higher in the beginning of test and decreased rapidly close to the hydration-end as depicted in Figure 7. As a result, the water content increased rapidly at section X1 with the initiation of hydration (see Fig. 4a). For the farther sections i.e. X2 and X3, the water migration process can be depicted as diffusion process where the concentration gradient is equivalent to the water content gradient.

In the further analysis of results, the water volume infiltrated into the soil sample was computed from the volumetric water content isochrones (Fig. 8). These isochrones were obtained from the transient water content measurements by assuming a constant dry density (1.85 Mg/m^3) along the height of soil sample. Prior to initiate the hydration, the mean volumetric water content

along the height of soil sample was equal to 16.65 % (i.e., 9 × 1.85). With the initiation of hydration, soil total suction dissipated rapidly to zero at the bottom-most layer of the sample (i.e., z = 0 mm). The corresponding volumetric water content (39.13 %) at z = 0 mm was calculated from the measured water content during the post-experimental investigations and assigned to all the time steps. The transient water content measurements were not performed at the top-end (i.e., z = 300 mm), the reported values in Figure 8 were obtained from the linear interpolation. The water volume infiltrated into the soil sample was computed at different time intervals and compared with the injected water volume, which was measured during the test (Fig. 9). A good agreement can be observed between the computed and the measured data. A decrease in the flow rate due to the progressive decrease of water potential gradient is evident in Figure 9.

The fact of having the same relative humidity corresponding to two different water content values at section X1 and X2 (see Fig. 4b) along with the different gravimetric water contents at full saturation stage (i.e., 21.15% at the bottom-end and 18% at section X1) indicate the redistribution of porosity, particularly close to the hydration-end. In the past, several researchers have observed the hydration induced porosity redistribution in the compacted bentonite (e.g., Monroy et al., 2010; Romero et al., 2011; Villar et al., 2014). For instance, Villar et al. (2014) analyzed the samples of compacted bentonite blocks, which were subjected to isothermal (average temperature 16 °C) peripheral hydration for a period of 10.5 years. The post-mortem analyses indicated the increasing dry density from the periphery towards the inner sections. The porosity redistribution may lead to an error in the computation of degree of saturation based on the assumption of constant initial void ratio (i.e., 0.47 in the present case) particularly at the sections close to hydration-end. In the present case, degree of saturation larger than one was obtained at the

section X1 (50 mm from bottom end) at low suction values (see Fig. 5b), which may be attributed to the underestimation of the void ratio. Additionally, Jacinto et al. (2016) highlighted the effect of the density of water on the computed degree of saturation in the case of samples of expansive clays tested at constant volume condition. Villar and Lloret (2004) showed that the average density of water in saturated samples of compacted bentonite depends on the specimen density and gravimetric water content, and values higher than 1.05 Mg/m^3 and up to 1.22 Mg/m^3 were obtained for bentonite dry densities between 1.3 and 1.8 Mg/m^3.

5.2 Material swelling behavior

The measured axial and lateral total stresses data were analyzed together with the transient water content and relative humidity measurements to have a better understand the coupled hydro-mechanical behavior of compacted Calcigel bentonite-sand mixture. The axial total stress evolution at the bottom-end showed a good resemblance with the relative humidity and water content evolution at section X1. With the initiation of hydration, it increases rapidly to 1.1 MPa in 45 days and later showed a gradual increase before reaching to 1.68 MPa in 349 days. During the clay-water interaction, the bentonite-based materials swells due to crystalline swelling and osmotic/double layer swelling mechanisms (van Olphen, 1963; Madsen & Müller-Vonmoos, 1989). The relative importance of these two mechanisms varies depending on the nature of exchangeable cations (i.e., Na^+ or Ca^{+2}). For instance, Cases et al. (1997) found that the crystalline swelling during the adsorption was completed at a relative humidity of about 70 % in case of Ca-rich bentonite. On the other hand, Saiyouri et al. (2000, 2004) found that the crystalline swelling in Ca-rich bentonite completed at a suction of 4 MPa, when a transition in the interlayer spacing

from 1.56 nm (two monomolecular layers of water) to 1.86 nm (three monomolecular layers) took place. Ca-rich bentonite has a considerable range of stability with two molecular layer of water and it has substantially no expansion beyond an interlayer spacing of about 1.9 nm (Aylmore & Quirk, 1959). However, it may continue to accommodate more water on the particle's outer surfaces and result in to the inter-particle osmotic swelling (Madsen & Müller-Vonmoos, 1989; Segad et al., 2010).

In the present case, the initial relative humidity of Calcigel bentonite-sand mixture was 81 %. At the relative humidity of 80 %, two monomolecular layers of water (d001 spacing = 1.56 nm) exist in Ca-rich bentonites (Saiyouri et al., 2000, 2004). It signifies that the swelling of Calcigel bentonite-sand mixture (50:50) exposed to water (within 45 days) is due to the crystalline swelling which occurs because of the transition of interlayer spacing from two monomolecular to three monomolecular layers of water. As a result, the rapid increase in the axial swelling pressure at the bottom-end was observed during the test. With the further hydration, the sample accommodated more water on the surfaces of clay particles. As the interlayer space cannot exceed beyond 1.9 nm (Aylmore & Quirk, 1959), the gradual increase in the swelling pressure beyond the crystalline swelling was due to the osmotic phenomenon.

The aggregate swelling in the lower elements during the hydration compressed the upper elements, which was measured by the top load cell. Under a confined condition and at equilibrium, it may be anticipated that the measured axial stress at both ends of the sample are equal. However, the axial stress developed at the top end of the sample was not transmitted towards the bottom of the sample. This can be attributed to the following factors, such as (i) dissimilar compressibility

characteristics along the height of the sample due to the difference in the water content along the height, (ii) the presence of construction joints meant for installing the pressure transducers, (iii) the side frictional resistance between the sample and the PVDF rings, and (iv) the composite nature of the sample due to the presence of sensors that created complex stress-deformation characteristics of the system. As shown in Figure 6a, the axial total stress measured at top end increases continuously and exceeds the bottom load cell measurement at time t = 238 days as depicted by a point P. This signifies the initiation of the swelling of the upper block under the influence of above-mentioned factors. Börgesson et al. (1995) investigated the effect of interfacial friction on the swelling-compression behavior of compacted bentonite-based specimens and found that the lateral stresses (corresponding to the normal stresses towards the rock surface) are higher than the stress in the swelling direction. It signifies that the swelling pressure is likely to be lower towards the sealing plug than on top of the canister due to the friction between the buffer and the rock.

The measured total stresses in lateral direction along the height of soil sample were higher than the axial total stresses measured at the top and bottom ends, which reveals the heterogeneity in the transient hydration process and its effect on the soil stiffness. In further analysis, the lateral stress profiles (Fig. 10) and the measured lateral stress vs. soil total suction at respective measurement sections (Fig. 11) are presented. Figure 10 indicates the elastoplastic behavior close to the hydration end (i.e., section X1); while the measurement sections X2 and X3 depict the elastic swelling behavior. In the initial phase of hydration, the elastic swelling is dominant at section X1 as a result the swelling pressure increased rapidly to 1.75 MPa in 15 days. With the progressive hydration, the suction reduction leads to a decrease in the apparent preconsolidation pressure and

consequently sample undergoes to plastic deformation, which is evident from the radial total stress measurements at section X1. In addition to the heterogeneity in the transient hydration process, the presence of technical/construction joints meant for installing the sensors also affect the soil stiffness. In the present case, the lateral total stress measurements were performed with a cylindrical piston (dia. = 20 mm) and a load cell assembly (Fig. 2). These pistons were kept in contact with the sample at sections X1, X2 and X3 during the installation process. In the axial direction, top and bottom load cells measure the soil response during transient hydration process in the presence of interfacial friction (b/w soil sample and cell wall) and the technical voids, which provide a higher stiffness of the system in the lateral direction as compared to that in the axial direction. Hence, the transient hydration of the compacted bentonite-sand mixture under the applied hydraulic gradient involves various complex processes, such as soil swelling, interaction between different soil layers, and induces the heterogeneity in the sample condition. The physical state of soil sample before and after the test is shown in Figure 12, which depicts the hydration-induced heterogeneity in the sample as a function of distance from the hydration-end.

5.3 Soil water retention behavior

Figure 13a shows the soil total suction vs. the measured transient water content and Figure 13b depicts the soil total suction vs. degree of saturation for sections X1, X2 and X3 along the height of soil sample. Soil total suction values were deduced from the relative humidity and temperature measurements using the Kelvin's equation. Whereas, the degree of saturation values were computed from the transient water content measurements with an assumption of a constant void ratio (0.47) along the height of soil sample. The transient data in Figure 13 were compared

with the data from an elementary test on the compacted bentonite-sand specimen (dia. = 50 mm; height = 20 mm) having identical initial conditions (i.e., dry density = 1.85 Mg/m^3 and water content = 9 %). In elementary test, the as-compacted samples were subjected to wetting under constant volume condition by reducing the soil suction in stage wise manner.

The transient measurements (soil suction vs. gravimetric water content) in Figure 13a show a good agreement with the elementary test results. On the other hand, Fig. 13b (soil suction vs. degree of saturation) shows some variation in the transient data at section X1and in the elementary test data at higher relative humidity levels. The observed variation is mainly due to the assumption of a constant void ratio along the height, which leads to an overestimation of the degree of saturation in case of expansive soil particularly at the higher relative humidity levels. The fact of having the same relative humidity corresponding to two different water content values at section X1 and X2 (see Fig. 4b) along with the different gravimetric water contents i.e., 21.15% at the bottom end and 18% at section X1 at full saturation stage clearly indicate the porosity redistribution during the hydration. Additionally, the effect of the density of water on the computed degree of saturation in the case of samples of expansive clays tested at constant volume condition may also affect the computed values of degree of saturation (Jacinto et al., 2016).

6. Conclusions

A water infiltration test was conducted with a compacted Calcigel bentonite-sand mixture (50:50) at room temperature to investigate the material response under an applied hydraulic gradient relevant to the hydration of backfill material at nuclear waste repository. The effect of

ground water geochemistry was not considered in this research work. Hence, the transient hydration of the compacted blocks as a backfill material was performed by supplying the distilled water from the bottom-end of sample. The test was performed with an innovative column-type experimental device under a constant volume condition. The sensors and monitoring instruments facilitated the transient measurements of water content, relative humidity, temperature and total stresses in both lateral direction (along the height of soil sample) and in the axial direction (at both the ends of soil sample) during the hydration process. The following conclusions were drawn from the study.

- The evolution of measured parameters (i.e., water content and relative humidity) and the computed parameters (i.e., soil total suction and degree of saturation) exhibited the effect of distance from the wetting-end on the rate of saturation. A progressive decrease in the water potential gradient was observed during the hydration process, which was sharp at the beginning of the test but became smoother with the time close to the hydration end. Consequently, the section of the sealing/backfill material close to the host rock saturates faster than the interior sections during the initial phase of hydration. The simultaneous measurements of water content and relative humidity along the sample height revealed the redistribution of porosity particularly for the sections close to hydration-end at the higher relative humidity level. In the present study, the test was performed for a period of 349 days and the material did not achieve full saturation. The post-experimental investigations revealed the heterogeneous distribution of measured and computed parameters along the height of soil sample during the hydration process.

- The axial and lateral total stress measurements indicated the effect of heterogeneity in the transient hydration process and the resulting non-homogeneous soil stiffness along the height of soil sample. In addition to the heterogeneity in the transient hydration process, the presence of technical/construction joints meant for installing the sensors also affect the soil stiffness in the axial and lateral direction. The measured axial stresses at the top and bottom ends of the sample were different, which can be attributed to the side frictional resistance offered by the sample rings and the presence of sensors that created a composite sample with varying stress-deformation characteristics. In the field, the interfacial friction between the host-rock and the compacted blocks may affect the swelling pressure distribution, as a results the swelling pressure is likely to be lower towards the sealing plug than on top of the canister.

- Considering the application of embedded pressure transducers, the transient measurements revealed that the selection of embedded pressure transducers i.e., dimensions, measurement capacity and the installation procedure should be considered carefully during the design phase of experimental device.

- The data pertaining to the soil water retention behavior (i.e., soil suction vs. gravimetric water content) indicated that the saturation of compacted blocks took place under the under constant volume condition. However, some variation in the transient data and in the elementary test results (soil suction vs. degree of saturation showed) were observed at section X1 (close to hydration end) at lower suction range. It may be attributed to the underestimation of void ratio particularly close to the hydration end during the computation

of degree of saturation with an assumption of constant void ration along the sample height.

Finally, the newly designed column-type experimental device shows a promising performance and has potential to be used for a variety of tests relevant to the coupled thermo-hydro-mechanical behavior of expansive soils under repository relevant boundary conditions.

ACKNOWLEDGMENT

The presented study has been performed within the framework of the project "Transient water transport in expansive soils under coupled hydraulic, mechanical and thermal boundary conditions: Experimental and numerical study'' funded by German Research Council (DFG, project No. SCHA 675/17-1). The authors are grateful to DFG for the financial support.

References

Alonso, E., Alcoverro, J., Coste, F., Malinsky, L., Merrien-Soukatcho, V., Kadiri, I., Nowak, T., Shao, H., Nguyen, T., Selvadurai, A. et al., 2005. The FEBEx benchmark test: case definition and comparison of modelling approaches. International Journal of Rock Mechanics and Mining Sciences. 5 (42), 611-638.

Åkesson, M., Jacinto, A. C., Gatabin, C., Sanchez, M., Ledesma, A., 2009. Bentonite THM behavior at high temperatures: experimental and numerical analysis. Geotechnique. 59 (4), 307–318.

Aylmore, L., Quirk, J., 1959. Swelling of clay-water systems. Nature 183, 1752-1753.

Börgesson, L., Chijimatsu, M., Fujita, T., Nguyen, T. S., Rutqvist, J., Jing, L., 2001. Thermo-Hydro-Mechanical characterization of a bentonite-based buffer material by laboratory tests and numerical back analyses. International Journal of Rock Mechanics and Mining Sciences. 38, 95–104.

Börgesson, L., Sanden, T., Johannesson, L.E., Hernelind, J., 1995. Modelling of the physical behaviour of water saturated clay barriers. laboratory tests, material models and finite element application. SKB Technical Report 95-20.

Cases, J., Bérend, I., François, M., Uriot, J., Michot, L., Thomas, F., 1997. Mechanism of adsorption and desorption of water vapor by homoionic montmorillonite: 3, the Mg^{2+}, Ca^{2+}, and Ba^{3+} exchanged forms. Clays and Clay Minerals. 45(1), 8-22.

Cuevas, J., Villar, M.V., Fernández, A.M., Gómez, P., Martín, P.L., 1997. Pore waters extracted from compacted bentonite subjected to simultaneous heating and hydration. Applied Geochemistry. 12, 473–481.

DIN18123 (1996), Soil investigation and testing – determination of grain-size distribution.

Gatabin, C., Billaud, P., 2005. Bentonite THM mock-up experiments: sensors data report. Tech. rep., CEA, Rapport NT-DPC/SCCME 05-300-A. CEA, Paris.

Gens, A., Sánchez, M., Guimarães, L.D.N., Alonso, E., Lloret, A., Olivella, S., Villar, M., Huertas, F., 2009. A full-scale in situ heating test for high-level nuclear waste disposal: observations, analysis and interpretation. Geotechnique. 59 (4), 377-399.

Jacinto, A.C., Ledesma, A., Demagistri, A., 2016. Effect of the clay-water interaction in the hydration of compacted bentonite used in engineered barriers. Geomechanics for Energy and the Environment. 8, 52-61.

Jobmann, M., Flügge, J., Gazul, R., Hammer, J., Herold, P., Krone, J., Kuate Simo, E., Kühnlenz, T., Laggiard, E., Lommerzheim, A., Meleshyn, A., Müller, C., Rübel, A., Wolf, J., Zhao, H., 2017. Investigation on long-term safety aspects of a radioactive waste repository in a diagenetic clay formation. Technical report, GRS BGR DBE TEC.

Jobmann, M., Flügge, J., Hammer, J., Herold, P., Krone, J., Kühnlenz, T., Li, S., Lommerzheim, A., Meleshyn, A., Wolf, J., 2015. Site-specific evaluation of safety issues for high-level waste disposal in crystalline rocks. Technical report, GRS BGR DBE TEC.

Madsen, F., Müller-Vonmoos, M., 1989. The swelling behaviour of clays. Applied Clay Science. 4, 143-156.

Martín, P. L., Barcala, J.M., 2005. Large-scale buffer material test: mock-up experiment at CIEMAT. Engineering Geology. 81, 298–316.

Monroy, R., Zdravkovic, L., Ridley, A., 2010. Evolution of microstructure in compacted London clay during wetting and loading. Geotechnique. 60 (2), 105-119.

Pintado, X., Ledesma, A., Lloret, A., 2002. Back analysis of thermo-hydraulic bentonite properties from laboratory tests. Engineering Geology. 64, 91–115.

Pusch, R., Kasbohm, J., 2001. Can the water content of highly compacted bentonite be increased by applying a high water pressure? Swedish Nuclear Fuel and Waste Management Co., Technical Report No. 01-33.

Romero, E., Della Vecchia, G., Jommi, C., 2011. An insight into the water retention properties of compacted clayey soils. Geotechnique. 61(4), 313-328.

Rothfuchs, T., Jockwer, N., Miehe, R., Zhang, C. L., 2005. Self-sealing barriers of clay/mineral mixtures in a clay repository: Sb experiment in the mont terri rock laboratory. Technical report, Gesellschaft für Anlagen-und Reaktorsicherheit (GRS).

Saba, S., Cui, Y., Tang, A.M., Barnichon, J., 2014. Investigation of the swelling behaviour of compacted bentonite–sand mixture by mock-up tests. Canadian Geotechnical Journal. 51, 1399–1412.

Saiyouri, N., Hicher, P.Y., Tessier, D., 2000. Microstructural approach and transfer water modelling in highly compacted unsaturated swelling clays. Mechanics of Cohesive-frictional Materials: An International Journal on Experiments, Modelling and Computation of Materials and Structures. 5(1), 41-60.

Saiyouri, N., Tessier, D., Hicher, P.Y., 2004. Experimental study of swelling in unsaturated compacted clays. Clay Minerals, 39(4), 469-479.

Schanz, T., Nguyen-Tuan, L., Datcheva, M., 2013. A column experiment to study the thermo-hydro-mechanical behavior of expansive soils. Journal of Rock Mechanics and Rock Engineering. 46, 1287–1301.

Segad, M., Jonsson, B., Åkesson, T., Cabane, B., 2010. Ca/Na montmorillonite: structure, forces and swelling properties. Langmuir. 26(8), 5782-5790.

Tripathy, S., Thomas, H.R., Bag, R., 2015. Geoenvironmental application of bentonites in underground disposal of nuclear waste: characterization and laboratory tests. Journal of Hazardous, Toxic, and Radioactive Waste. 21 (1), 1–12.

van Olphen, H., 1963. An introduction to clay colloid chemistry. 1st edition, John Wiley & Sons, New York London Sydney Toronto.

Villar, M., Campos, R., Gutiérrez-Nebot, L., 2014. Long-term performance of engineered barrier systems PEBS. EB experiment Laboratory post-mortem analyses report, the Seventh Framework Programme of the European Atomic Energy Community (Euratom), DELIVERABLE (D2.1-7), 1-34.

Villar, M.V., Martín, P.L., Barcala, J.M., 2005. Modification of physical, mechanical and hydraulic properties of bentonite by thermo-hydraulic gradients. Engineering Geology. 81, 284–297.

Villar, M., Lloret, A., 2004. Influence of temperature on the hydro-mechanical behaviour of a compacted bentonite. Applied Clay Science. 26 (1), 337 - 350.

Yong, R.N., Mohamed, A.M.O., Shooshpasha, I., Onofrei, C., 1997. Hydro-Thermal performance of unsaturated bentonite sand buffer material. Engineering Geology. 47, 351–365.

Wang, Q., Cui, Y.J., Tang, A.M., Barnichon, J.D., Saba, S., Ye, W.M., 2013. Hydraulic conductivity and microstructure changes of compacted bentonite/ sand mixture during hydration. Engineering Geology. 164, 67–76.

List of Tables

TABLE 1. Geotechnical properties of soil tested.

Properties	Values
Calcigel bentonite	
Specific gravity	2.80
Liquid limit (%)	180
Plastic limit (%)	43-45
Shrinkage limit (%)	18-21
Plasticity index	135-137
Cation Exchange Capacity (meq/100g)	74
Montmorillonite content (%)	60-70
Specific surface area (m^2/g)	400
Sand	
Specific gravity	2.65
D10 (mm)	0.25
D30 (mm)	0.40
D60 (mm)	0.70

TABLE 2. Details of the monitoring sensors and instruments used with the device.

Measuring parameter and sensor type	Nos.	Installation remark	Measurement specifications	Accuracy
Temperature (Pt100)	5	At sections X1, X2, and X3 (3 nos.), at top and bottom plugs (2 nos.); Sensor dia. = 3 mm, embedment length = 10 mm.	- 40 to 200 °C	(0.1 + 0.0017×|t|) °C
Relative humidity (VAISALA HMT337 with heating option)	3	In closed vapor chambers at sections X1, X2, and X3. Additional Pt100 probe embedded in the sample up to 10 mm.	0 to100 % RH	± (1.5 + 0.015 × reading) % RH
Water content (IMKO PICO-32)	3	At sections X1, X2, and X3.	0 to 70 %	± 2 % for 0 - 40 % ± 3 % for 40 - 70 %
Lateral stress (OMEGA Engg.: LCM-203)	3	At sections X1, X2, and X3.	5 kN	± 0.3 % including nonlinearity, hysteresis, and repeatability
Axial stress (OMEGA Engg.: LCM-402)	2	At top and bottom ends	100 kN	Same as above in lateral stress
Axial pressure (KYOWA-BEC pressure transducer)	2	At the interfaces between blocks S1-S2, and S2-S3.	1 MPa	± 0.03 MPa (incl. nonlinearity and hysteresis with additional ± 0.4 % / °C due to T effect
Thermostats (Huber Ministat 230 and CC-202)	2	External unit.	20 to 95 °C	Temperature stability = ± 0.02 °C
Data logger (Graphtech-820)	1	External unit	20 channels	-

List of Figure

Fig. 8: Volumetric water content isochrones at different selected time intervals.

Fig. 9: Measured and calculated infiltrated-water volume into the soil sample.

Fig. 10: Lateral total stress profiles along the height of soil sample.

Fig. 11: Lateral total stress vs. soil suction for measurement sections X1, X2 and X3.

Fig. 12: Material physical state before and after the test.

Fig. 13: Transient soil water retention curves, (a) water content vs. soil suction and (b) degree of saturation vs. soil suction for measurement sections X1, X2 and X3.

List of Figures

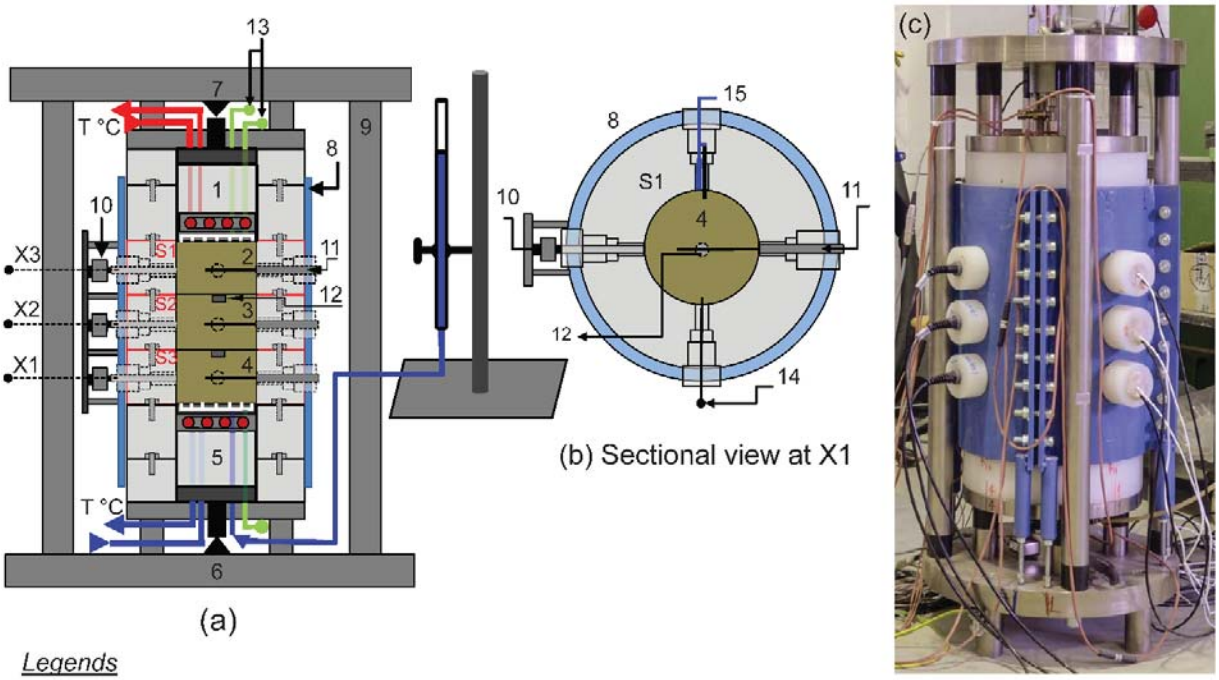

Legends

1 = Top plug; 2, 3, 4 = Compacted blocks; 5 = Bottom plug; 6 = Bottom load cell; 7 = Top load cell; 8 = Confining cell; S1, S2 and S3 = Sample rings; 9 = Rigid frame; 10 = Radial load cells; 11 = TDRs; 12 = Pressure transducers; 13 = Top air vent; 14 = Pt100 sensor; 15 = RH sensor with additional Pt100 probe; X1, X2 and X3 = Measurement sections; = heating/cooling coil.

Fig. 1: Constructional details of the newly designed column-type experimental set-up, (a) and (b) vertical and horizontal sectional views, and (c) a photograph of the device.

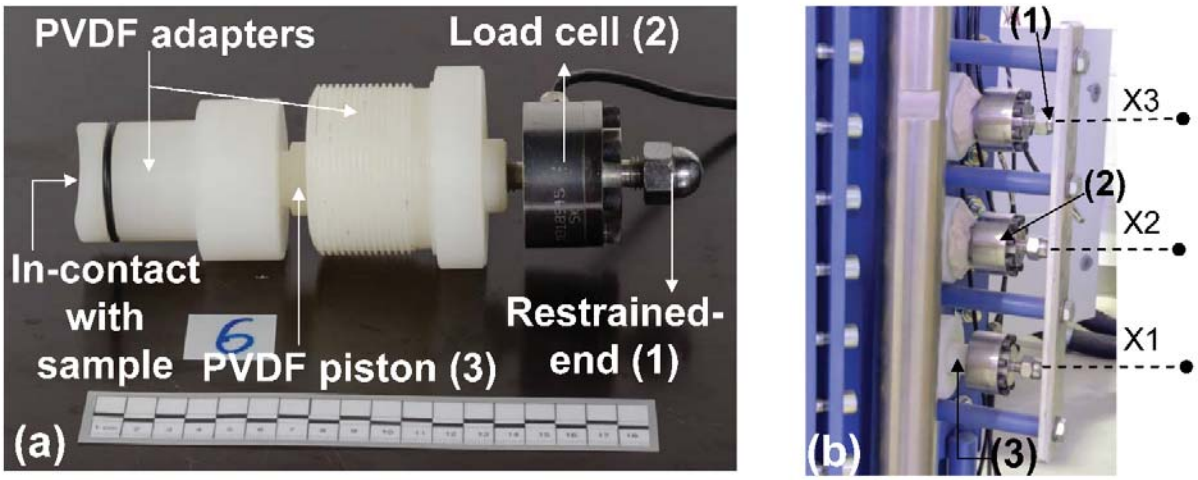

Fig. 2: Lateral load cell installation details, (a) load cell along with accessories and (b) installation at measurement sections X1, X2 and X3 along the height of soil sample.

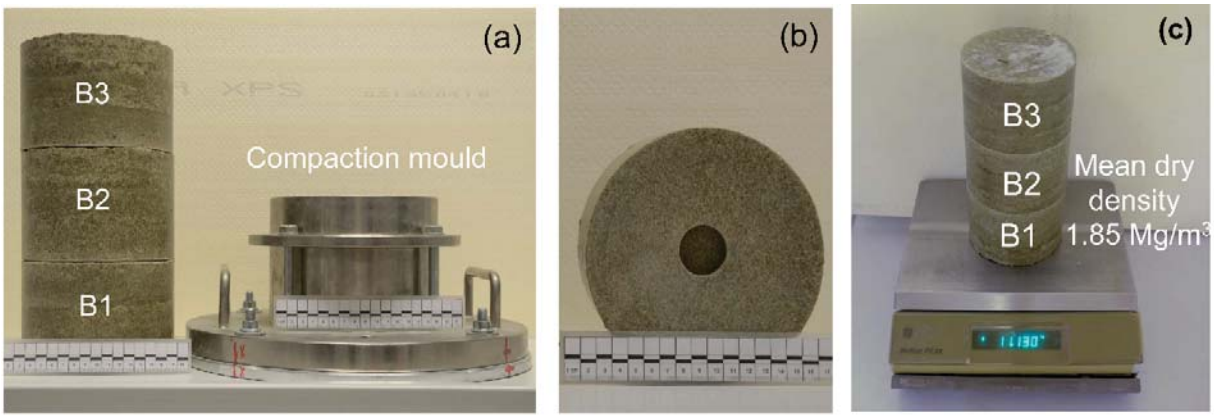

Fig. 3: Sample preparation using static uniaxial compaction, (a) compacted blocks and compacting mould, (b) seating space for KYOWA pressure transducer and (c) average mean density.

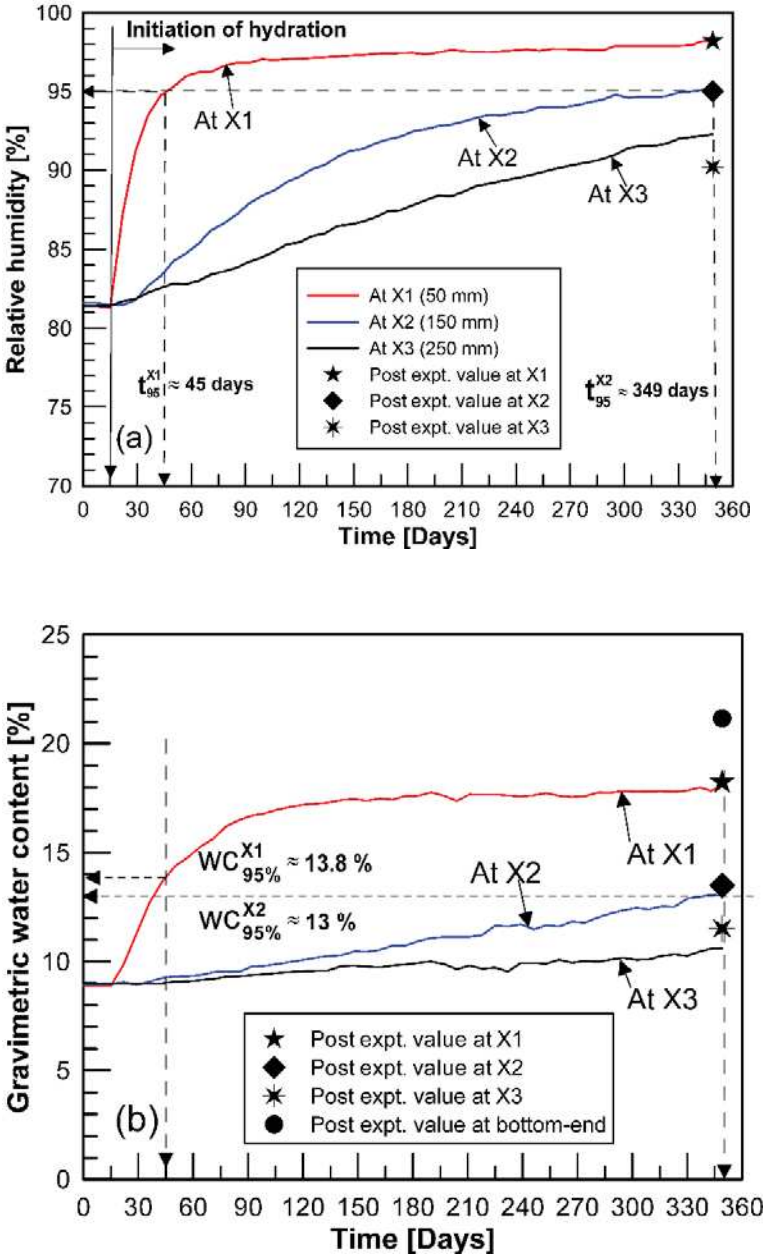

Fig. 4: (a) Elapsed time vs. relative humidity and (b) elapsed time vs. water content plots at salient levels along the height of the sample.

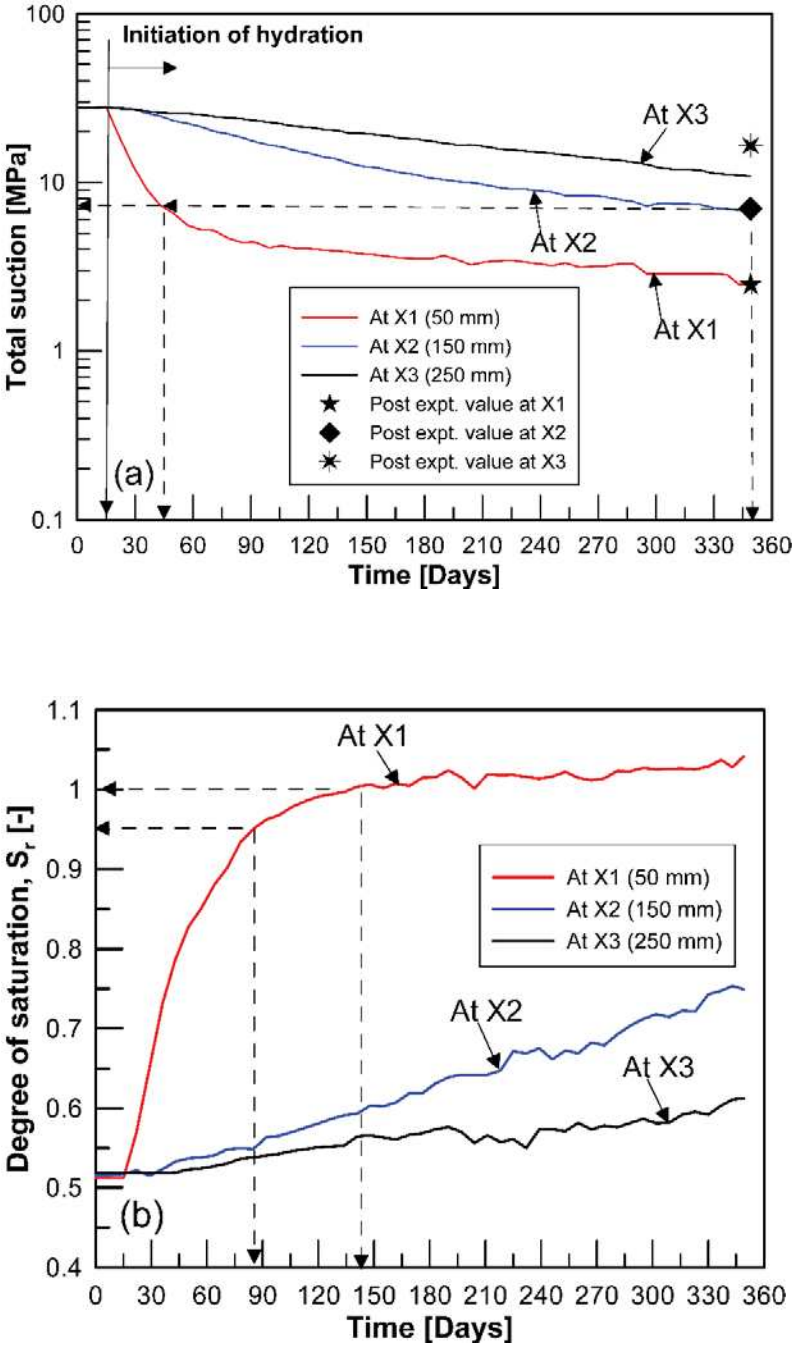

Fig. 5: (a) Elapsed time vs. soil total suction and (b) elapsed time vs. degree of saturation plots at salient levels along the height of the sample.

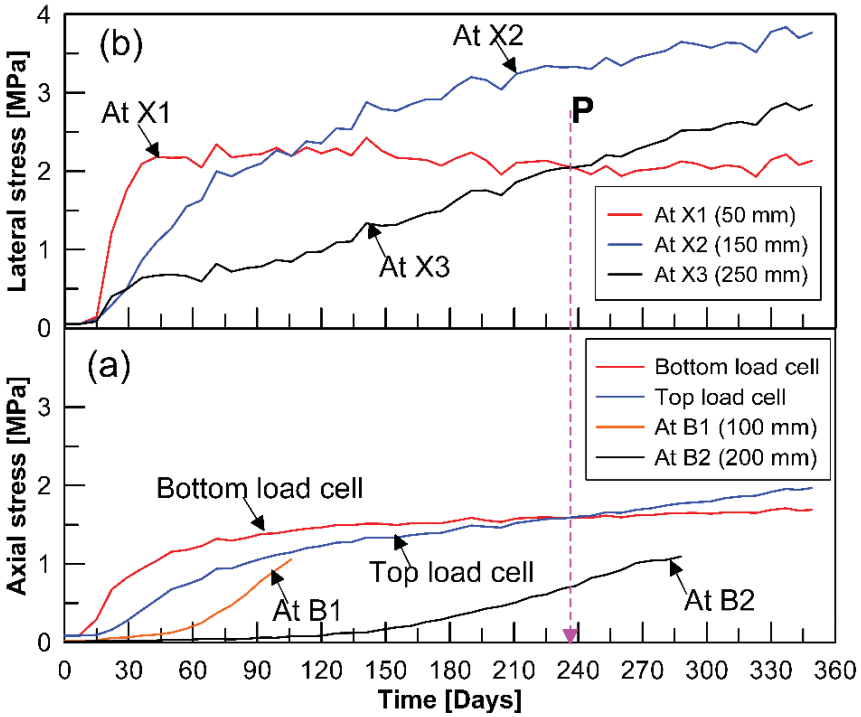

Fig. 6: Evolution of total stress, (a) axial total stress measurements with time and (b) radial total stress measurements with time.

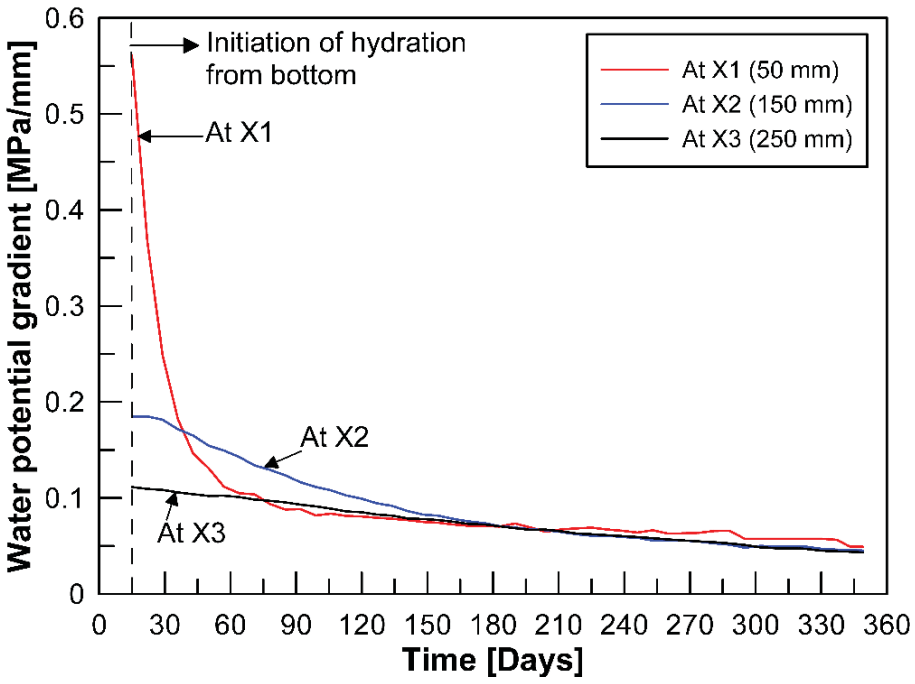

Fig. 7: Water potential gradient vs. elapsed time.

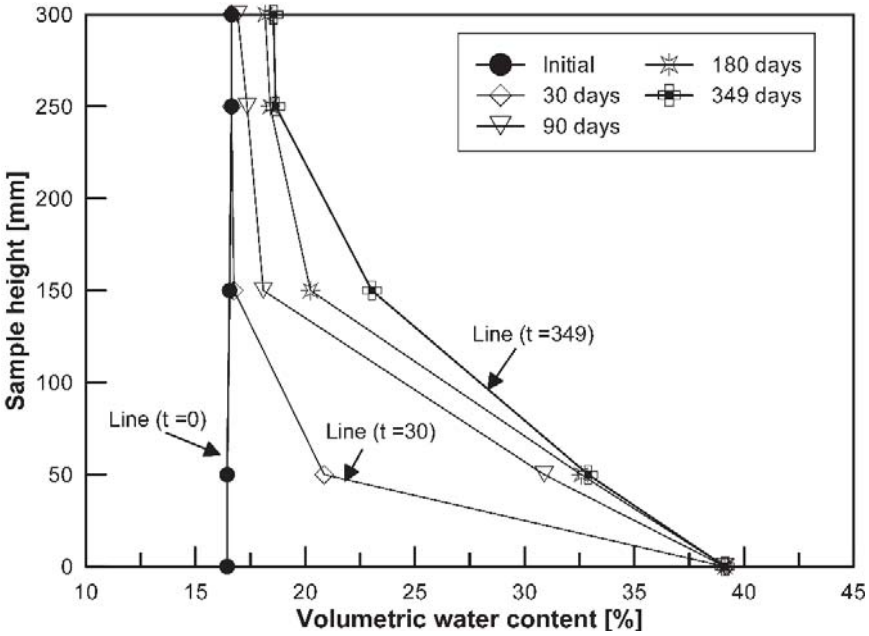

Fig. 8: Volumetric water content isochrones at different selected time intervals.

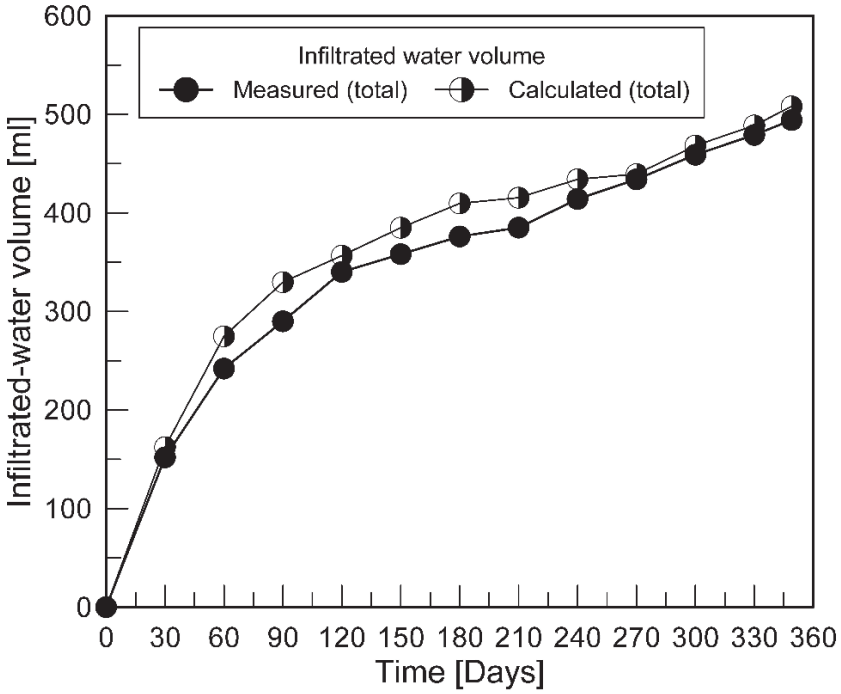

Fig. 9: Measured and calculated infiltrated-water volume into the soil sample.

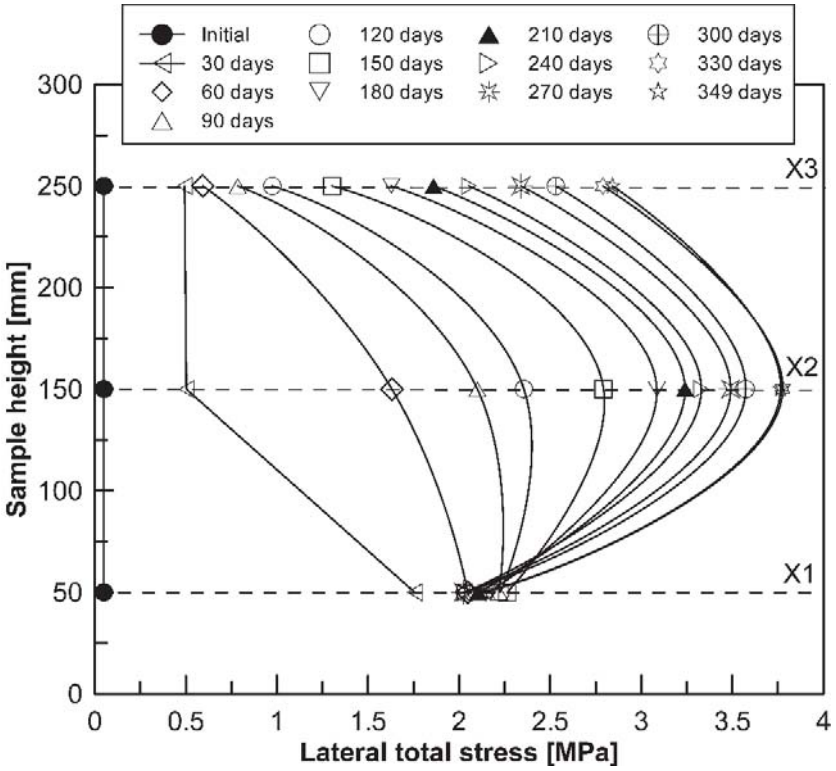

Fig. 10: Lateral total stress profiles along the height of soil sample.

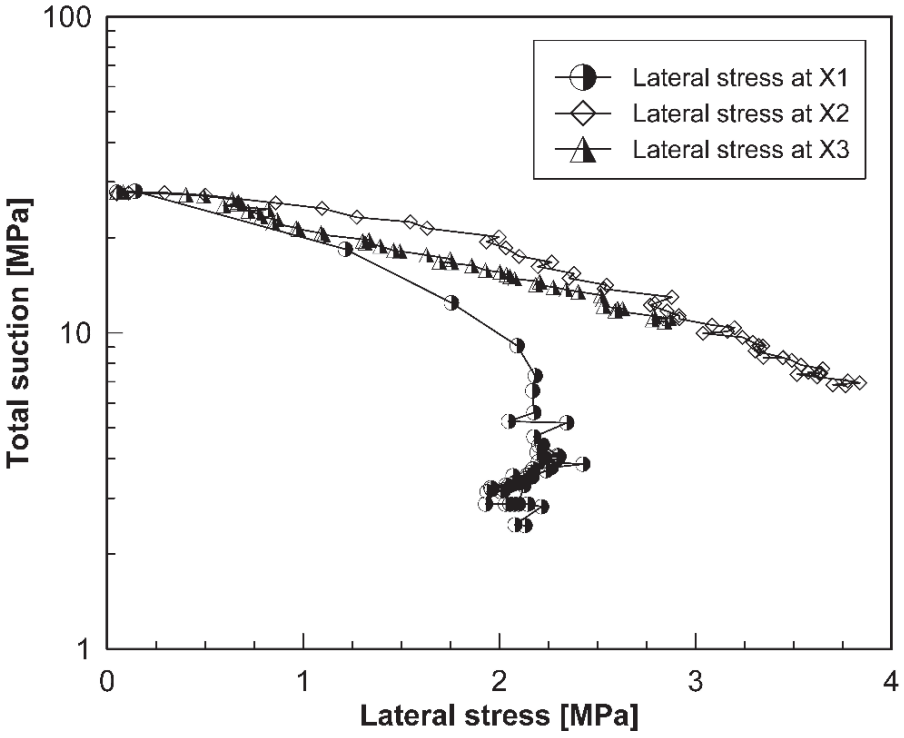

Fig. 11: Lateral total stress vs. soil suction for measurement sections X1, X2 and X3.

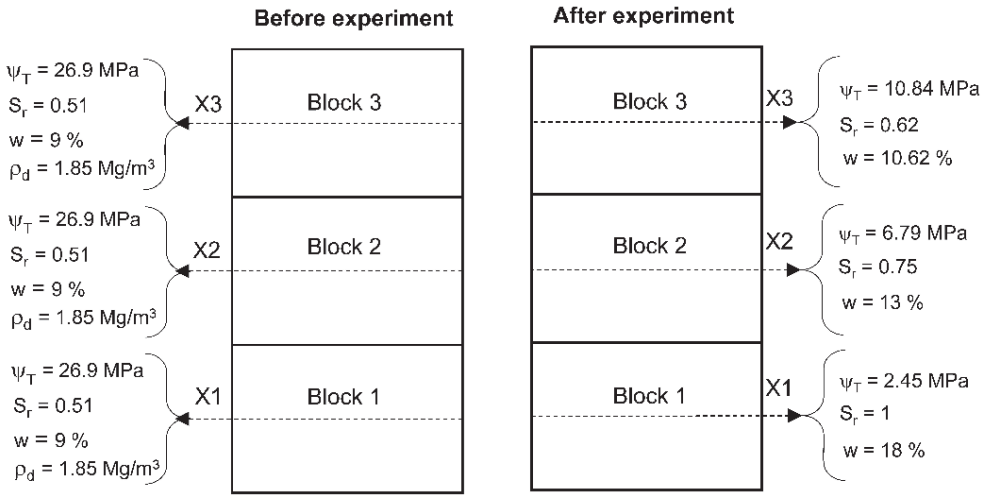

Fig. 12: Material physical state before and after the test.

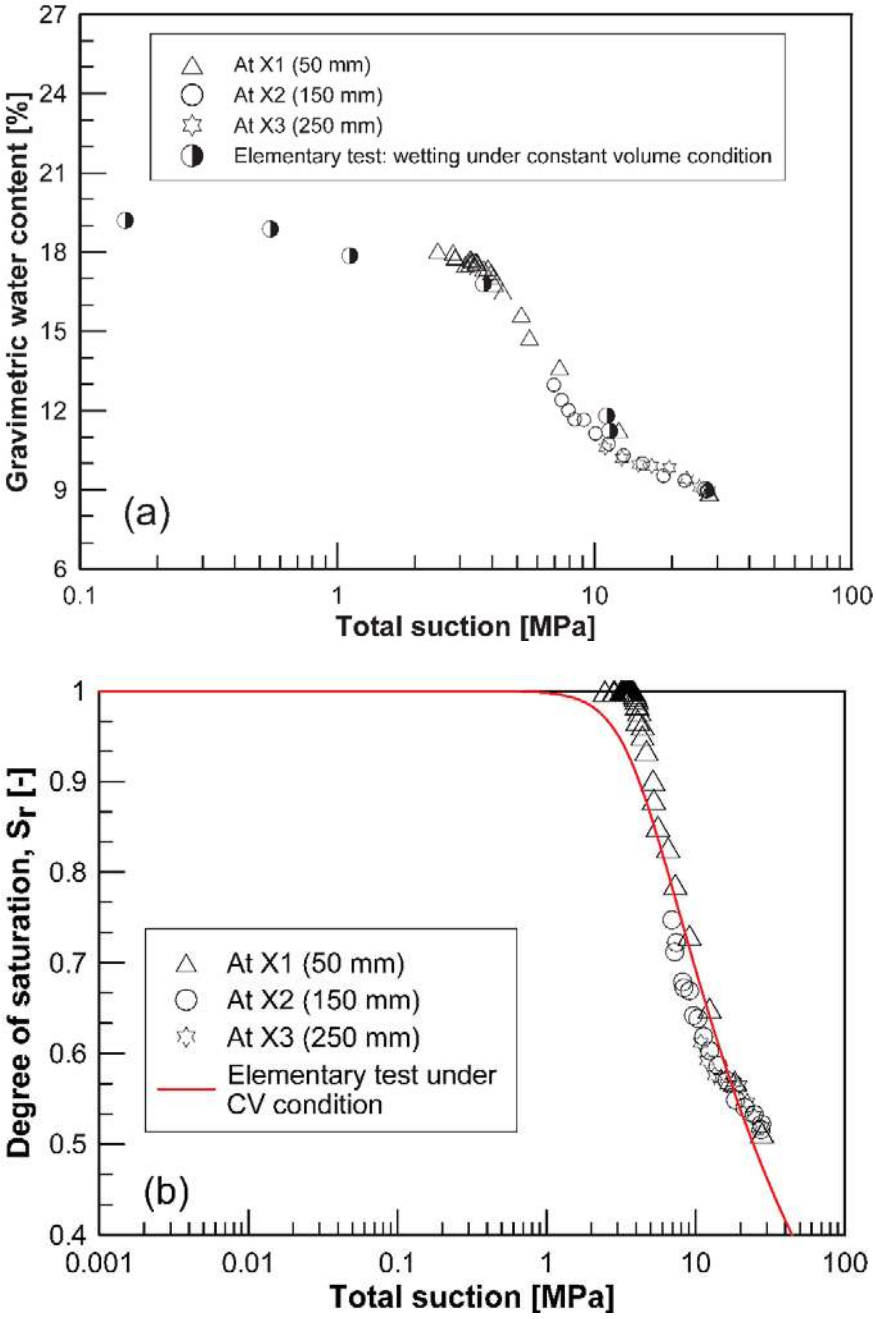

Fig. 13: Transient soil water retention curves, (a) water content vs. soil suction and (b) degree of saturation vs. soil suction for measurement sections X1, X2 and X3.